GEOPHYSICS, VOL. 89, NO. 3 (MAY-JUNE 2024); P. S267–S274, 14 FIGS., 1 TABLE.
10.1190/GEO2023-0374.1

DOI:10.1190/geo2023-0374.1

Target-oriented least-squares reverse time migration with Marchenko redatuming and double focusing: Field data application

Aydin Shoja[1], Joost van der Neut[2], and Kees Wapenaar[1]

ABSTRACT

Recently, the focus of reflection seismologists has shifted to applications for which a high-resolution image of the subsurface is required. Least-squares reverse time migration (LSRTM) is a common tool used to compute such images. Even so, its high computational costs have led seismologists to use target-oriented LSRTM for imaging only a small target of interest within a larger subsurface block. Redatuming the data to the upper boundary of the target of interest is one approach to target-oriented LSRTM, but many redatuming methods cannot account for multiple scattering within the overburden. We apply a target-oriented LSRTM algorithm that integrates Marchenko redatuming and double focusing to a field data set. This redatuming method accounts for all orders of multiple scattering in the overburden, thus improving the accuracy of target-oriented LSRTM. Moreover, we determine the effectiveness of a double-focusing algorithm in reducing the data size by decreasing spatial and temporal dimensions of the model and the data. The algorithm's performance is evaluated using field data acquired in the Norwegian Sea. The numerical results indicate that the target-oriented LSRTM algorithm with Marchenko double-focusing can reduce the internal multiple effects and increase the resolution of the resulting image.

INTRODUCTION

Seismic imaging and inversion are a set of techniques used by geophysicists to estimate parameters related to wave propagation, such as reflectivity, velocity, and density, within the earth's subsurface. A network of sources and receivers is positioned on the earth's surface to produce and record seismic waves, from which these parameters are determined. Geophysicists typically assume a subsurface model that consists of a background model (m_0) for long wavelengths and a perturbation model for short wavelengths (δm), based on a weak-scattering assumption (Claerbout, 1985; Schuster, 2017). The primary objective of seismic imaging is to generate a structural image of the short-wavelength perturbation model (δm).

Reverse time migration (RTM) is a popular method among different imaging techniques because it can produce high-resolution images and better handle complex geologic structures (Baysal et al., 1983; McMechan, 1983; Zhou et al., 2018; Zhang et al., 2019). RTM creates images by crosscorrelating the forward-propagated wavefield and its back-propagated counterpart based on the Born approximation. However, improving the resolution and quality of RTM images is possible by inverting the Lippmann-Schwinger integral under the Born approximation for the perturbation model with a least-squares algorithm (Tang, 2009; Liu et al., 2016; Dutta et al., 2017; Kaur et al., 2020; Huang, 2023). This inversion process is known as least-squares RTM (LSRTM).

However, LSRTM is a computationally expensive algorithm (Tang, 2009; Dai et al., 2012; Herrmann and Li, 2012; Farshad and Chauris, 2021). To reduce the computational cost of LSRTM, one can restrict the model's dimensions by focusing on a small area inside the big block of the subsurface model. To compute the image of this smaller region, the wavefield on the upper boundary of this region is needed at least. The process of computing the wavefield on the boundary of this target from surface-recorded data is called redatuming (Valenciano et al., 2006; Haffinger et al., 2013; Ravasi et al., 2016; Willemsen et al., 2016; Yuan et al., 2017; Zhao and Sen, 2018; Guo and Alkhalifah, 2020; Huang et al., 2020; Biondi et al., 2023). One prominent redatuming technique is Marchenko redatuming (Wapenaar et al., 2014, 2021; Diekmann and Vasconcelos, 2021).

Marchenko redatuming (Wapenaar et al., 2014, 2021; van der Neut et al., 2015a, 2015b; Dukalski and de Vos, 2017; Wapenaar and Staring, 2018) can create virtual receivers on the boundary of the

Manuscript received by the Editor 22 June 2023; revised manuscript received 24 November 2023; published ahead of production 23 February 2024; published online 17 April 2024.
[1]Delft University of Technology, Department of Geoscience and Engineering, Delft, The Netherlands. E-mail: s.m.a.shoja@tudelft.nl (corresponding author); c.p.a.wapenaar@tudelft.nl.
[2]Delft University of Technology, Department of Imaging Physics, Delft, The Netherlands. E-mail: jrvanderneut@yahoo.com.

DOI:10.1190/geo2023-0374.1

target of interest while accounting for all orders of internal multiple scattering effects and reflections. Because Marchenko redatuming and Green's functions retrieval are powerful tools, researchers use them to address seismic imaging and inversion issues (Cui et al., 2018, 2020; Zhang et al., 2019; Diekmann et al., 2023). Moreover, it is possible to perform a double-sided redatuming using Marchenko focusing functions. Double-sided redatuming creates virtual sources in addition to virtual receivers at the boundary of the target. The process of double-sided redatuming also is called double focusing (Staring et al., 2018; Shoja et al., 2023). Marchenko double-focused wavefields account for all orders of internal multiples generated inside the overburden, enabling us to create images with less impact from internal multiples. Moreover, Marchenko double focusing compacts the data's time axis, reducing its size even more.

This paper combines the Marchenko double focusing and target-oriented LSRTM algorithm to create high-resolution artifact-free images of a marine data set from the Vøring region in the Norwegian Sea. First, we review the theory of target-oriented LSRTM with Marchenko double focusing, which is fully developed and is validated with synthetic models by Shoja et al. (2023). Second, we apply this algorithm to a marine data set, and finally, we discuss the results and conclude the paper.

THEORY

Least-squares RTM

Dai et al. (2012) show that classical RTM can be derived from the Born approximation of seismic reflection data. In the Born approximation, the incident wavefield (P^{inc}) can be estimated using the background Green's function. The perturbation model is expressed as $\delta m = ((1/c^2) - (1/c_0^2))$, where c represents the medium velocity and c_0 represents the background velocity. This equation links δm to the scattered data in the frequency domain (P^{scat}) through a linear relation (Born et al., 1999; Schuster, 2017; van den Berg, 2021):

$$P^{\text{scat}}_{\text{pred}}(\mathbf{x}_r,\mathbf{x}_s,\delta m,\omega)=\frac{\omega^2}{\rho_0}\int_V G_0(\mathbf{x}_r,\mathbf{x},\omega)\delta m(\mathbf{x})P^{\text{inc}}(\mathbf{x},\mathbf{x}_s,\omega),d\mathbf{x}. \tag{1}$$

The integral in equation 1 is computed throughout the model's volume (V). Here, $P^{\text{inc}}(\mathbf{x},\mathbf{x}_s,\omega) = G_0(\mathbf{x},\mathbf{x}_s,\omega)W(\omega)$. Moreover, ω is the angular frequency, W is the source signature, G_0 is the Green's function computed in the background model (c_0), ρ_0 is the background density, and $P^{\text{scat}}_{\text{pred}}$ is the scattered predicted data. The subscripts r and s indicate the receiver and source, respectively. This equation can be expressed in an operator format as follows:

$$P^{\text{scat}}_{\text{pred}}(\mathbf{x}_r,\mathbf{x}_s,\delta m,\omega) = \mathcal{L}\delta m, \tag{2}$$

where $\mathcal{L}$ is the forward Born operator.

The standard method of RTM involves obtaining an approximate perturbation model by taking the adjoint of $\mathcal{L}$ and applying it to the observed scattered data:

$$\delta m^{\text{mig}}(\mathbf{x}) = \mathcal{L}^\dagger P^{\text{scat}}_{\text{obs}}. \tag{3}$$

Because the adjoint of this kernel is merely an approximation of its inverse, the resolution of the perturbation model obtained through this process is limited.

To tackle the problem of limited resolution, scholars have adopted a least-squares strategy in which the adjoint operator ($\mathcal{L}^\dagger$) is substituted with a damped least-squares solution (Marquardt, 1963; Dai et al., 2012; Dutta et al., 2017):

$$\delta m^{\text{mig}} = [\mathcal{L}^\dagger\mathcal{L} + \epsilon]^{-1}\mathcal{L}^\dagger P^{\text{scat}}_{\text{obs}}, \tag{4}$$

where $\mathcal{L}^\dagger\mathcal{L}$ is the Hessian matrix and ϵ is a damping factor. Unfortunately, calculating the Hessian matrix ($\mathcal{L}^\dagger\mathcal{L}$) and its inverse is computationally infeasible. As an alternative, an iterative algorithm that minimizes the L2 norm of the discrepancy between the observed and predicted data often is used to update the perturbation model:

$$C(\delta m) = \frac{1}{2}\|P^{\text{scat}}_{\text{pred}}(\delta m) - P^{\text{scat}}_{\text{obs}}\|_2^2. \tag{5}$$

One potential way to tackle this optimization problem is by using a conjugate gradient algorithm (Nocedal and Wright, 2006). In LSRTM, the background velocity model ($c_0(\mathbf{x})$) is not changed, and only the perturbation model (δm) is updated, resulting in the Green's functions of equation 1 being calculated only once. To learn more about LSRTM, please see Schuster (2017).

Marchenko redatuming and double focusing

Marchenko redatuming is an innovative data-driven technique that can recover the Green's function generated by a source at the surface and recorded by a virtual receiver just above the target area's surface, including all orders of multiple-scattered events. This method only requires the reflection response at the surface and a smooth background velocity model of the overburden capable of predicting the direct arrival from the surface to the redatuming level.

The following coupled Marchenko-type representations are solved iteratively to retrieve the Green's functions at the redatuming level (Wapenaar et al., 2014):

$$G^-_{\text{Mar}}(\mathbf{x}_v,\mathbf{x}_r,\omega) = \int_{\mathcal{D}_{\text{acq}}} R(\mathbf{x}_r,\mathbf{x}_s,\omega)f_1^+(\mathbf{x}_s,\mathbf{x}_v,\omega)d\mathbf{x}_s - f_1^-(\mathbf{x}_r,\mathbf{x}_v,\omega) \tag{6}$$

and

$$G^+_{\text{Mar}}(\mathbf{x}_v,\mathbf{x}_r,\omega) = -\int_{\mathcal{D}_{\text{acq}}} R(\mathbf{x}_r,\mathbf{x}_s,\omega)f_1^-(\mathbf{x}_s,\mathbf{x}_v,\omega)^*d\mathbf{x}_s + f_1^+(\mathbf{x}_r,\mathbf{x}_v,\omega)^*, \tag{7}$$

where $\mathcal{D}_{\text{acq}}$ represents the acquisition surface where $\mathbf{x}_s$ and $\mathbf{x}_r$ are situated, and G^-_{Mar} and G^+_{Mar} denote the upgoing and downgoing components of the Marchenko redatumed Green's function, respectively (see Figure 1a and 1b). In addition, $f_1^-(\mathbf{x}_s,\mathbf{x}_v,\omega)$ and $f_1^+(\mathbf{x}_s,\mathbf{x}_v,\omega)$ denote the upgoing and downgoing parts of the focusing function, respectively, with the subscript v denoting a virtual point situated on the redatuming level denoted by $\mathcal{D}_{\text{tar}}$. Furthermore, $R(\mathbf{x}_r,\mathbf{x}_s,\omega)$ refers to the dipole response of the medium at the acquisition surface, and it is related to the upgoing Green's function at the acquisition surface (G^-) via the following relationship (Wapenaar and Berkhout, 1989):

DOI:10.1190/geo2023-0374.1

$$R(\mathbf{x}_r,\mathbf{x}_s,\omega)=\frac{\partial_{3,s}G^{-}(\mathbf{x}_r,\mathbf{x}_s,\omega)}{\frac{1}{2}i\omega\rho(\mathbf{x}_s)}. \tag{8}$$

The partial derivative in the downward direction taken at $\mathbf{x}_s$ is denoted by $\partial_{3,s}$. This partial vertical derivative is computed in the frequency-wavenumber domain by multiplying the wavefield by ik_z, where k_z is the vertical wavenumber. Here, $\rho(\mathbf{x}_s)$ is the density at $\mathbf{x}_s$. It is important to remove horizontally propagating waves and surface-related multiples before inserting $R(\mathbf{x}_r,\mathbf{x}_s,\omega)$ into equations 6 and 7. The detailed derivation of these integrals and their solution for computing the focusing functions and Green's functions can be found in Wapenaar et al. (2014) and Thorbecke et al. (2017).

The preceding equations correspond to single-sided redatuming. To perform a double-sided redatuming, a convolution operation on the upgoing and downgoing parts of the Marchenko redatumed Green's function is proposed by Staring et al. (2018). This operation involves filtering the downgoing focusing function in a multidimensional manner:

$$G_{\mathrm{df}}^{-,+}(\mathbf{x}_v,\mathbf{x}_v',\omega)=\int_{\mathcal{D}_{\mathrm{acq}}}G_{\mathrm{Mar}}^{-}(\mathbf{x}_v,\mathbf{x}_r,\omega)\mathcal{F}_1^{+}(\mathbf{x}_r,\mathbf{x}_v',\omega)d\mathbf{x}_r \tag{9}$$

and

$$G_{\mathrm{df}}^{+,+}(\mathbf{x}_v,\mathbf{x}_v',\omega)=\int_{\mathcal{D}_{\mathrm{acq}}}G_{\mathrm{Mar}}^{+}(\mathbf{x}_v,\mathbf{x}_r,\omega)\mathcal{F}_1^{+}(\mathbf{x}_r,\mathbf{x}_v',\omega)d\mathbf{x}_r, \tag{10}$$

where

$$\mathcal{F}_1^{+}(\mathbf{x}_r,\mathbf{x}_v',\omega)=\frac{\partial_{3,r}f_1^{+}(\mathbf{x}_r,\mathbf{x}_v',\omega)}{\frac{1}{2}i\omega\rho(\mathbf{x}_r)}. \tag{11}$$

Here, the vertical derivative is taken with respect to $\mathbf{x}_r$, which is computed similar to $\partial_{3,s}$, as discussed above equation 8. Equations 9 and 10 use superscripts to indicate the direction of propagation at the receiver and source locations, respectively. The term df represents double focused. This process is referred to as "Marchenko double focusing."

The Marchenko double-focusing technique yields two Green's functions, namely a downgoing ($G_{\mathrm{df}}^{+,+}$) and an upgoing ($G_{\mathrm{df}}^{-,+}$) Green's function (Figure 1c and 1d). The downgoing Green's function consists of a band-limited delta function and interactions between the target and the overburden. Here, $G_{\mathrm{df}}^{-,+}$ can be interpreted as the continuation of propagation of $G_{\mathrm{df}}^{+,+}$ through the target and recording the upgoing part of it at the redatuming level. This upgoing wavefield includes interactions between the target and the overburden on the source side. In contrast, the conventional double-focusing approach involves using the inverse of the direct arrival of the transmission response of the overburden instead of the downgoing Marchenko focusing function. However, this approach cannot predict and remove the multiples generated by the overburden. In subsequent sections, the term double focusing is a general expression that refers to these approaches, and it is explicitly mentioned when a distinction between the methods is necessary.

Target-oriented LSRTM by Marchenko double focusing

The theory of the method is fully described by Shoja et al. (2023). Here, we give a brief explanation of the theory. The following integral is the base for target-oriented LSRTM by Marchenko double focusing:

$$\hat{P}_{\mathrm{pred}}^{\mathrm{scat}}(\mathbf{x}_{\mathrm{vr}}',\mathbf{x}_{\mathrm{vs}}',\delta m,\omega)=\frac{\omega^2}{\rho_0}\int_{\mathcal{V}}\hat{G}_0(\mathbf{x}_{\mathrm{vr}}',\mathbf{x},\omega)\delta m(\mathbf{x})P_{\mathrm{df}}^{\mathrm{inc}}(\mathbf{x},\mathbf{x}_{\mathrm{vs}}',\omega)d\mathbf{x}, \tag{12}$$

where $\mathcal{V}$ is the target volume, $\mathbf{x}$ is a point inside the target, and $\mathbf{x}_{\mathrm{vs}}'$ and $\mathbf{x}_{\mathrm{vr}}'$ are the virtual source and virtual receiver locations on the upper boundary of the target, respectively. Moreover,

$$P_{\mathrm{df}}^{\mathrm{inc}}(\mathbf{x},\mathbf{x}_{\mathrm{vs}}',\omega)=\int_{\mathcal{D}_{\mathrm{tar}}}\frac{\partial_{3,\mathrm{vs}}G_0(\mathbf{x},\mathbf{x}_{\mathrm{vs}},\omega)}{\frac{1}{2}i\omega\rho(\mathbf{x}_{\mathrm{vs}})}G_{\mathrm{df}}^{+,+}(\mathbf{x}_{\mathrm{vs}},\mathbf{x}_{\mathrm{vs}}',\omega)W(\omega)d\mathbf{x}_{\mathrm{vs}} \tag{13}$$

and

$$\hat{G}_0(\mathbf{x}_{\mathrm{vr}}',\mathbf{x},\omega)=\int_{\mathcal{D}_{\mathrm{tar}}}\Gamma(\mathbf{x}_{\mathrm{vr}}',\mathbf{x}_{\mathrm{vr}},\omega)G_0(\mathbf{x}_{\mathrm{vr}},\mathbf{x},\omega)d\mathbf{x}_{\mathrm{vr}}, \tag{14}$$

where

$$\Gamma(\mathbf{x}_{\mathrm{vr}}',\mathbf{x}_{\mathrm{vr}},\omega)=\int_{\mathcal{D}_{\mathrm{acq}}}G_d^{+}(\mathbf{x}_{\mathrm{vr}}',\mathbf{x}_s,\omega)^{-1}G_d^{+}(\mathbf{x}_{\mathrm{vr}},\mathbf{x}_s,\omega)d\mathbf{x}_s \tag{15}$$

is a point-spread function that acts as a band limitation filter on the predicted data. In equation 15, G_d^{+} is the first arrival of the Green's function between the target boundary and the surface. For a complete derivation of the preceding equations and an analysis of the effects of the point-spread function ($\Gamma(\mathbf{x}_{vr}',\mathbf{x}_{vr},\omega)$), we refer to Shoja et al. (2023). Thus, the new cost function is

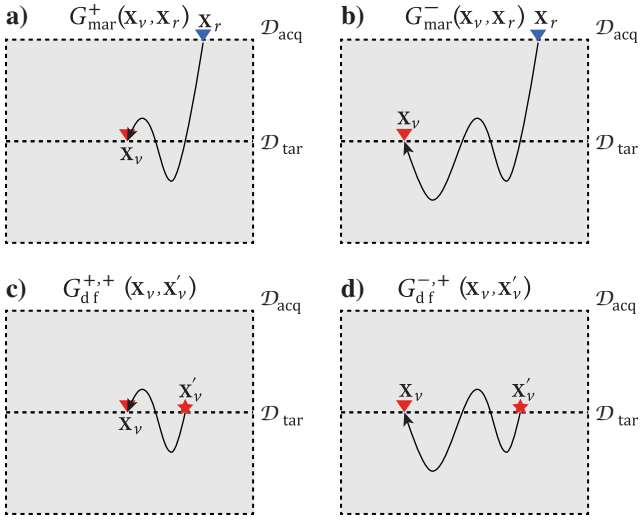

Figure 1. The Green's functions resulting from Marchenko redatuming and double focusing: (a) downgoing part of Marchenko Green's function, (b) upgoing part of Marchenko Green's function, (c) downgoing Marchenko double-focused Green's function, and (d) upgoing Marchenko double-focused Green's function.

DOI:10.1190/geo2023-0374.1

$$C(\delta m) = \frac{1}{2}\|\hat{P}^{\text{scat}}_{\text{pred}}(\delta m) - \hat{P}^{\text{scat}}_{\text{obs}}\|_2^2, \tag{16}$$

where

$$\hat{P}^{\text{scat}}_{\text{obs}} = G^{-,+}_{\text{df}}(\mathbf{x}'_{\text{vr}}, \mathbf{x}'_{\text{vs}}, \omega)W(\omega). \tag{17}$$

We solve equation 16 with a conjugate gradient algorithm.

FIELD DATA EXAMPLE

In a previous paper (Shoja et al., 2023), target-oriented LSRTM with double focusing is tested on synthetic models. Here, we apply this method to a field data set.

Field data explanation

This part of the paper shows the results of the Marchenko-based target-oriented LSRTM on a field data set provided by Equinor, which was acquired in the Norwegian Sea in 1994. The water bottom depth is 1.5 km, which is sufficiently deep to separate the free-surface multiple reflections from the primary and internal multiple reflections. The field data set contains 399 shot gathers with 180 traces per gather, and the spatial sampling of sources and receivers is 25 m. The field data set was processed using the method proposed by Davydenko and Verschuur (2018), which involved muting the direct wave, estimating near-offset traces through the parabolic Radon transform (Kabir and Verschuur, 1995), compensating for 3D effects by multiplying with $\sqrt{t}$, and deconvolving the source wavelet. Source-receiver reciprocity also is applied to create offsets in the positive direction to prepare the data set for the estimation of primaries through sparse inversion method to remove free-surface multiples (van Groenestijn and Verschuur, 2009). After source-receiver reciprocity, each gather contains 371 receivers. Because it is not possible to recover the traces after the last shot with source-receiver reciprocity, dummy traces are added in this part of the data to have an equal number of traces in each shot gather. Table 1 shows the acquisition parameters, and Figure 2 shows the acquisition geometry of this data set. Adding reciprocal traces also is in line with having regularly sampled data for the Marchenko scheme. Van IJsseldijk and Wapenaar (2020) study the possibility of using data with irregular sampling. We apply a time gain of $1.73e^{1.3t}$ to the reflection response as recommended by Brackenhoff et al. (2019) to compensate for the absorption effect. However, with this scaling function, the Marchenko redatuming procedure does not sufficiently reduce the multiple reflections energy for imaging. An incorrect scaling function can result in more artifacts (van der Neut et al., 2015a). Thus, we multiplied the reflection response already scaled with the aforementioned scaling function, using a range of values to adjust it for imaging. Then, we measured the L2 norm of the double-focused gather to find the value that produces the minimum energy (van der Neut et al., 2015b; Brackenhoff, 2016). Figure 3 shows the L2 norm of the double-focused gather against the values we use. According to Figure 3, we choose value 10, which results in an adjusted scaling factor of $17.3e^{1.3t}$ for the original (nonscaled) reflection response.

Figure 4 shows the surface reflection response after preprocessing, with a source located at $\mathbf{x}_s = (5000\text{ m}, 0\text{ m})$. We choose two different targets inside the medium.

Table 1. Acquisition parameters for the data set.

Parameter	Value
Number of source positions	399
Source spacing	25 m
First source position	5000 m
Final source position	14,950 m
Number of receiver positions per source	180
Receiver spacing	25 m
Minimum source-receiver offset	150 m
Maximum source-receiver offset	4625 m
Number of time samples	2001
Sampling rate	0.004 s
High-cut frequency	90 Hz

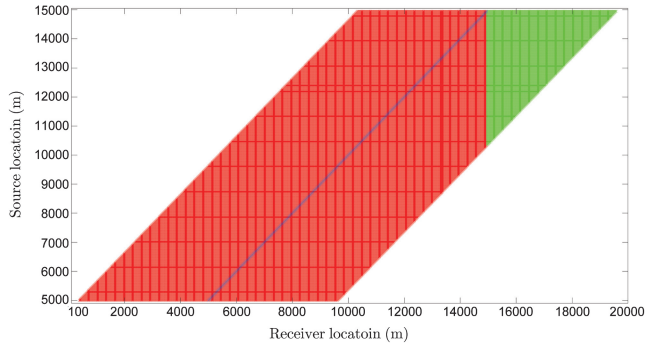

Figure 2. The acquisition geometry of the data set. Blue crosses show the source locations, red crosses show the receiver locations, and green crosses show the dummy traces added after source-receiver reciprocity to have an equal number of receivers per shot. The receivers on the left side of the sources are the real ones, and the receivers on the right side are added by source-receiver reciprocity.

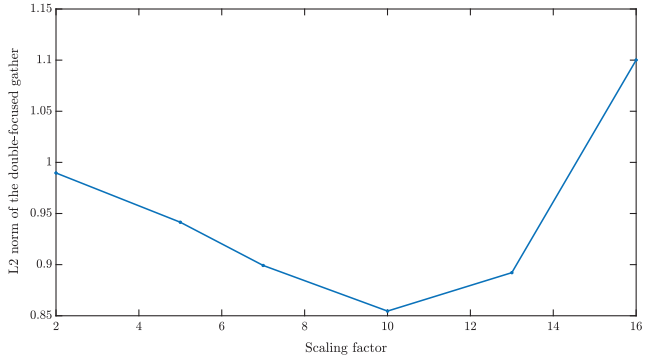

Figure 3. The L2 norm of the gather shown in Figure 6a against different scaling values.

LSRTM with double focusing

Target of interest 1.—Figure 5 shows the smooth velocity model provided by Equinor for migration. The red rectangle inside the velocity model indicates the target area, and the virtual source and receiver positions are at the upper boundary of this target area. We assume a constant density model for this study.

We apply the double-focusing algorithm to the field data for this target. For this, we define 241 virtual sources and 241 virtual receivers with a spacing of 12.5 m at a depth of 2500 m extending from 9000 m to 12,000 m over the upper boundary of the first target area. The upgoing wavefield resulting from double focusing is used as input for LSRTM and is called observed data in the following. Figure 6 shows the observed and predicted data next to the residuals of Marchenko double-focusing target-oriented LSRTM. Moreover, Figure 7 shows the same but for a conventional double-focusing approach. Conventional means using the inverse of the direct arrival between the target and the surface as the redatuming operator instead of the Marchenko focusing functions. The nonphysical noise in the data is caused by imperfect surface multiple elimination in this part of the data. The computational advantage of target-oriented LSRTM with double-focused data is twofold. First, this algorithm reduces the spatial dimension of the problem, and second, it reduces the temporal dimension of the problem as well. The original recording time of the data at the surface is 8 s, whereas the temporal length of the double-focused data is 0.5 s.

Figure 8 compares the LSRTM images of using Marchenko and conventional double-focused data as input. Figure 8 shows some improvements from using Marchenko double-focused wavefields compared with conventional double-focused ones. A comparison

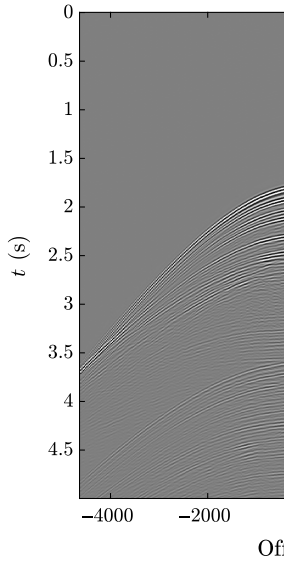

Figure 4. Reflection response with a source located at $\mathbf{x}_s = (5000\ \text{m}, 0\ \text{m})$. A Ricker wavelet with a dominant frequency of 30 Hz is convolved with the data for better visualization.

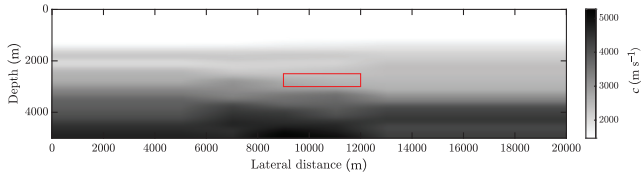

Figure 5. The smooth velocity model provided by Equinor for migration. The red rectangle inside the velocity model indicates the first target area. The virtual source and receiver positions are at the upper boundary of this target area.

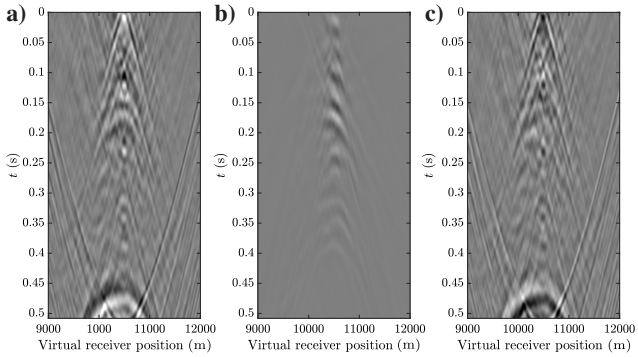

Figure 6. Marchenko double-focused data with a virtual source located at $\mathbf{x}_{vs} = (10{,}500\ \text{m}, 2500\ \text{m})$ and virtual receivers at the same depth as virtual sources. (a) Observed data obtained by Marchenko double focusing, (b) predicted data after 35 iterations of LSRTM, and (c) residuals after 35 iterations of LSRTM.

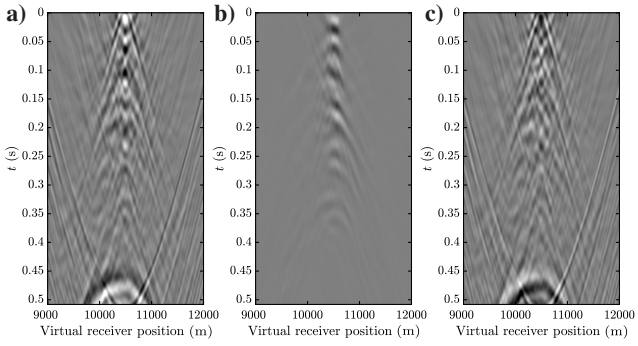

Figure 7. Conventional double-focused data with a virtual source located at $\mathbf{x}_{vs} = (10{,}500\ \text{m}, 2500\ \text{m})$. (a) Observed data obtained by conventional double focusing, (b) predicted data after 35 iterations of LSRTM, and (c) residuals after 35 iterations of LSRTM.

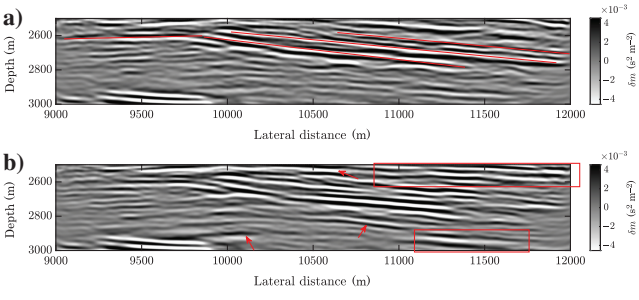

Figure 8. Comparison of images obtained with (a) Marchenko target-oriented LSRTM and (b) conventional target-oriented LSRTM. Red lines in (a) delineate some trends that are not visible in (b), and the red arrows and rectangles in (b) show some events that may be internal multiple reflection artifacts that are suppressed in (a).

DOI:10.1190/geo2023-0374.1

of our results with the results of Ypma and Verschuur (2013) and Davydenko and Verschuur (2018) confirms that the suppressed events are likely internal multiple reflections.

Moreover, Figure 9 compares the RTM and LSRTM images of Marchenko double-focused data as input. The LSRTM algorithm improved the quality of the image.

Target of interest 2.—Here, we choose another target. This target is located between depths of 2100 m and 2600 m and lateral extension from 7000 m to 10,000 m, as shown in Figure 10. Virtual sources and receivers are located at the upper boundary of this target area.

Figure 11 shows the observed and predicted data with corresponding residuals of the Marchenko double-focusing approach. Figure 12 shows the same for the conventional double-focusing approach.

Moreover, Figure 13 shows the LSRTM images of the target-oriented algorithm with Marchenko and conventional double focusing. The red arrows, the red rectangle, and the red ellipse indicate the internal multiple reflections that our method suppresses. Figure 14 shows the RTM and LSRTM images of the target-oriented algorithm with Marchenko double focusing. The LSRTM algorithm increases the quality and resolution of the image.

DISCUSSION

In the "Theory" section of this paper, we derive a target-oriented LSRTM algorithm based on double focusing that can significantly reduce the dimensions of the problem, which also reduces the computational costs of the LSRTM algorithm. We also integrate the Marchenko double-focusing algorithm with our target-oriented LSRTM algorithm to reduce the artifacts caused by internal multiple reflections.

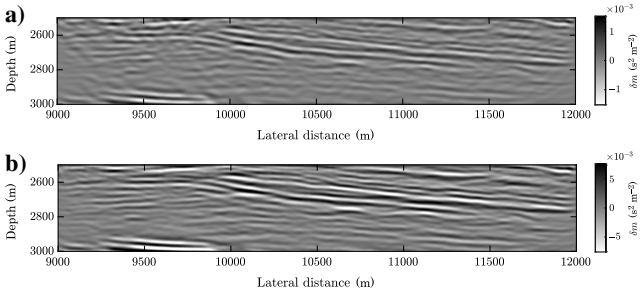

Figure 9. Comparison of images obtained with (a) Marchenko target-oriented RTM and (b) LSRTM of the first target.

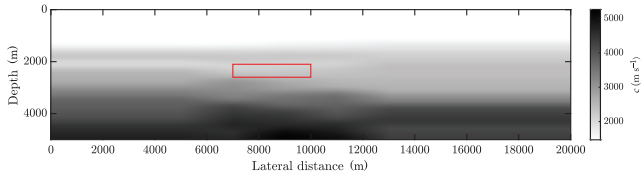

Figure 10. The smooth velocity model provided by Equinor for migration. The red rectangle inside the velocity model indicates the second target area, and the virtual source and receiver positions are at the upper boundary.

To demonstrate the advantages of our proposed algorithm, we applied it to a data set acquired by Equinor in the Norwegian Sea in 1994. We chose two different target zones. Figures 5 and 10 show our targets of interest embedded in the entire domain of the region. This spatial dimension reduction is to validate the first advantage that we mentioned previously. Figures 6a, 7a, 11a, and 12a show the double-focused data with a recording duration of 0.5 s, whereas the recording time of the original data is 8 s.

To move forward with our investigation, we showed the imaging results with double focusing for these targets. Figure 8 compares the conventional and Marchenko double-focusing target-oriented LSRTM imaging results. The first panel (Figure 8a) shows the LSRTM result of our proposed algorithm with Marchenko double-focused data, and the second panel (Figure 8b) shows the LSRTM results with conventional double-focused data. Comparing these two panels reveals that using Marchenko double-focused wavefields leads to better visualization of true events and fewer artifacts due to internal multiples, delineated by the lines and arrows in those panels. Moreover, Figure 9 shows the resolution and quality improvement of target-oriented LSRTM compared with target-oriented RTM with Marchenko double focusing.

The same discussion holds for the second target. Figure 13 shows a comparison between conventional and Marchenko double-focusing

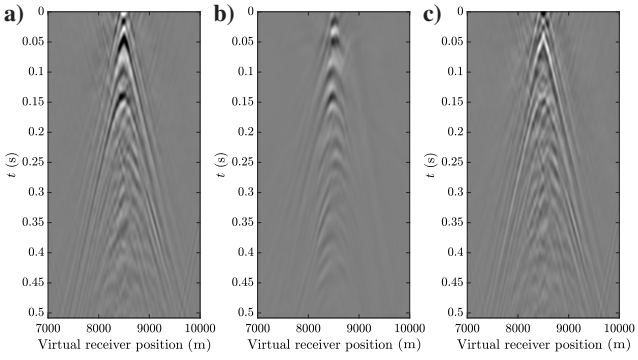

Figure 11. Marchenko double-focused data with a virtual source located at $\mathbf{x}_{vs} = (8500\ \text{m}, 2100\ \text{m})$ and virtual receivers at the same depth as virtual sources. (a) Observed data obtained by Marchenko double focusing, (b) predicted data after 35 iterations of LSRTM, and (c) residuals after 35 iterations of LSRTM.

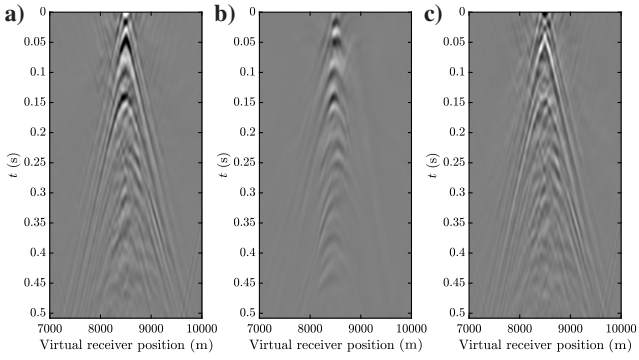

Figure 12. Conventional double-focused data with a virtual source located at $\mathbf{x}_{vs} = (8500\ \text{m}, 2100\ \text{m})$. (a) Observed data obtained by conventional double focusing, (b) predicted data after 35 iterations of LSRTM, and (c) residuals after 35 iterations of LSRTM.

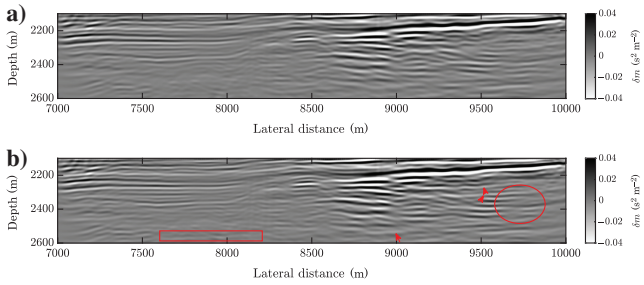

Figure 13. Comparison of images obtained with (a) Marchenko target-oriented LSRTM and (b) conventional target-oriented LSRTM. The red arrows, rectangle, and ellipse in (b) indicate some of the internal multiple reflection artifacts that are suppressed in (a).

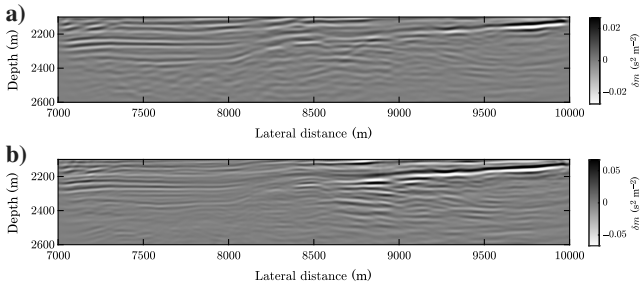

Figure 14. Comparison of images obtained with (a) Marchenko target-oriented RTM and (b) LSRTM of the second target.

target-oriented LSRTM images for which the internal multiple suppression is visible and indicated by arrows and an ellipse, and Figure 14 shows the RTM and LSRTM images of Marchenko double focusing. The quality and resolution of the image are increased noticeably. We use the internal multiple elimination results of Ypma and Verschuur (2013) and Davydenko and Verschuur (2018) as benchmarks for our results.

In the target areas, the double-focused gathers experience multiple flawed preprocessing stages that cannot be adequately explained by the forward modeling or the Marchenko approach. The nonphysical artifacts within the data primarily arise from incomplete surface multiple removal and the impact of 3D effects in 2D data sets. These spurious elements in the data have led to a substantial residual.

CONCLUSION

This paper discusses a target-oriented LSRTM algorithm based on double focusing. The advantages of this algorithm are (1) reduction of the spatial dimensions of the problem by choosing a smaller target of interest and (2) reduction of the temporal dimension of the problem by creating virtual sources and receivers at the boundary of the target, which leads to lower computational costs. One can opt for sophisticated redatuming algorithms such as Marchenko redatuming and double focusing to create virtual sources and receivers. The advantage of using Marchenko double focusing compared to a more conventional redatuming algorithm is the ability to predict the internal multiple reflections inside the overburden and a reduction of artifacts due to these multiple reflections.

The reason for choosing double focusing instead of multidimensional deconvolution (MDD) is to avoid another inversion step in our algorithm. MDD is an inversion process with its own uncertainties and associated errors. In contrast, the double focusing is a multidimensional convolution process with a stable output. As shown in previous studies and this paper, the predicted data, which use the double-focused downgoing wavefield at the boundary of the target, can predict the interactions between the target and the overburden and fit them to the double-focused observed data.

Present-day seismic imaging and inversion applications need more accurate and higher-resolution images. Computing higher-resolution images demands significant amounts of computational power and time. Thus, devising algorithms that can reduce this computational burden is essential. Our proposed target-oriented algorithm is not only able to greatly reduce the spatial and temporal dimensions of the problem but also can reduce the artifacts due to internal multiple reflections by integrating Marchenko double focusing with the LSRTM algorithm. Consequently, our algorithm enables us to create higher-resolution images with fewer artifacts at a lower computational cost.

ACKNOWLEDGMENTS

The authors would like to thank E. Verschuur for fruitful discussions and feedback. This work was supported by the European Union's Horizon 2020 Research and Innovation Program: European Research Council under grant no. 742703.

DATA AND MATERIALS AVAILABILITY

No data have been required for this paper.

REFERENCES

Baysal, E., D. D. Kosloff, and J. W. C. Sherwood, 1983, Reverse time migration: Geophysics, **48**, 1514–1524, doi: 10.1190/1.1441434.
Biondi, E., G. Barnier, B. Biondi, and R. G. Clapp, 2023, Target-oriented elastic full-waveform inversion through acoustic extended image-space redatuming: Geophysics, **88**, no. 3, R269–R296, doi: 10.1190/geo2022-0404.1.
Born, M., E. Wolf, A. B. Bhatia, P. C. Clemmow, D. Gabor, A. R. Stokes, A. M. Taylor, P. A. Wayman, and W. L. Wilcock, 1999, Principles of optics: Electromagnetic theory of propagation, interference and diffraction of light, 7th ed.: Cambridge University Press.
Brackenhoff, J., 2016, Rescaling of incorrect source strength using Marchenko redatuming: M.S. thesis, http://resolver.tudelft.nl/uuid:0f0ce3d0-088f-4306-b884-12054c39d5da, accessed 31 August 2016.
Brackenhoff, J., J. Thorbecke, and K. Wapenaar, 2019, Virtual sources and receivers in the real earth: Considerations for practical applications: Journal of Geophysical Research: Solid Earth, **124**, 11802–11821, doi: 10.1029/2019JB018485.
Claerbout, J. F., 1985, Imaging the earth's interior: BlackWell Scientific Publications.
Cui, T., J. Rickett, I. Vasconcelos, and B. Veitch, 2020, Target-oriented full-waveform inversion using Marchenko redatumed wavefields: Geophysical Journal International, **223**, 792–810, doi: 10.1093/gji/ggaa333.
Cui, T., J. E. Rickett, and I. Vasconcelos, 2018, Target-oriented waveform inversion: The Journal of the Acoustical Society of America, **144**, 1792–1792, doi: 10.1121/1.5067912.
Dai, W., P. Fowler, and G. T. Schuster, 2012, Multi-source least-squares reverse time migration: Geophysical Prospecting, **60**, 681–695, doi: 10.1111/j.1365-2478.2012.01092.x.
Davydenko, M., and D. J. Verschuur, 2018, Including and using internal multiples in closed-loop imaging — Field data examples: Geophysics, **83**, no. 4, R297–R305, doi: 10.1190/geo2017-0533.1.
Diekmann, L., and I. Vasconcelos, 2021, Focusing and Green's function retrieval in three-dimensional inverse scattering revisited: A single-sided Marchenko integral for the full wave field: Physical Review Research, **3**, 013206, doi: 10.1103/PhysRevResearch.3.013206.
Diekmann, L., I. Vasconcelos, and T. van Leeuwen, 2023, A note on Marchenko-linearised full waveform inversion for imaging: Geophysical Journal International, **234**, 228–242, doi: 10.1093/gji/ggad066.

Dukalski, M., and K. de Vos, 2017, Marchenko inversion in a strong scattering regime including surface-related multiples: Geophysical Journal International, **212**, 760–776, doi: 10.1093/gji/ggx434.
Dutta, G., M. Giboli, C. Agut, P. Williamson, and G. T. Schuster, 2017, Least-squares reverse time migration with local Radon-based preconditioning: Geophysics, **82**, no. 2, S75–S84, doi: 10.1190/geo2016-0117.1.
Farshad, M., and H. Chauris, 2021, Sparsity-promoting multiparameter pseudoinverse Born inversion in acoustic media: Geophysics, **86**, no. 3, S205–S220, doi: 10.1190/geo2020-0527.1.
Guo, Q., and T. Alkhalifah, 2020, Target-oriented waveform redatuming and high-resolution inversion: Role of the overburden: Geophysics, **85**, no. 6, R525–R536, doi: 10.1190/geo2019-0640.1.
Haffinger, P., A. Gisolf, and P. M. V. D. Berg, 2013, Towards high resolution quantitative subsurface models by full waveform inversion: Geophysical Journal International, **193**, 788–797, doi: 10.1093/gji/ggt021.
Herrmann, F. J., and X. Li, 2012, Efficient least-squares imaging with sparsity promotion and compressive sensing: Geophysical Prospecting, **60**, 696–712, doi: 10.1111/j.1365-2478.2011.01041.x.
Huang, X., 2023, Full wavefield inversion with multiples: Nonlinear Bayesian inverse multiple scattering theory beyond the Born approximation: Geophysics, **88**, no. 6, T289–T303, doi: 10.1190/geo2022-0604.1.
Huang, X., M. Jakobsen, K. Solberg Eikrem, and G. Nævdal, 2020, Target-oriented inversion of time-lapse seismic waveform data: Communications in Computational Physics, **28**, 249–275, doi: 10.4208/cicp.OA-2018-0143.
Kabir, M. N., and D. Verschuur, 1995, Restoration of missing offsets by parabolic Radon transform: Geophysical Prospecting, **43**, 347–368, doi: 10.1111/j.1365-2478.1995.tb00257.x.
Kaur, H., N. Pham, and S. Fomel, 2020, Improving the resolution of migrated images by approximating the inverse Hessian using deep learning: Geophysics, **85**, no. 4, WA173–WA183, doi: 10.1190/geo2019-0315.1.
Liu, Y., X. Liu, A. Osen, Y. Shao, H. Hu, and Y. Zheng, 2016, Least-squares reverse time migration using controlled-order multiple reflections: Geophysics, **81**, no. 5, S347–S357, doi: 10.1190/geo2015-0479.1.
Marquardt, D. W., 1963, An algorithm for least-squares estimation of nonlinear parameters: Journal of the Society for Industrial and Applied Mathematics, **11**, 431–441, doi: 10.1137/0111030.
McMechan, G. A., 1983, Migration by extrapolation of time-dependent boundary values: Geophysical Prospecting, **31**, 413–420, doi: 10.1111/j.1365-2478.1983.tb01060.x.
Nocedal, J., and S. J. Wright, 2006, Numerical optimization: Springer.
Ravasi, M., I. Vasconcelos, A. Kritski, A. Curtis, C. A. D. C. Filho, and G. A. Meles, 2016, Target-oriented Marchenko imaging of a North Sea field: Geophysical Journal International, **205**, 99–104, doi: 10.1093/gji/ggv528.
Schuster, G. T., 2017, Seismic inversion: SEG.
Shoja, A., J. van der Neut, and K. Wapenaar, 2023, Target-oriented least-squares reverse-time migration using Marchenko double-focusing: Reducing the artefacts caused by overburden multiples: Geophysical Journal International, **233**, 13–32, doi: 10.1093/gji/ggac438.
Staring, M., R. Pereira, H. Douma, J. van der Neut, and K. Wapenaar, 2018, Source-receiver Marchenko redatuming on field data using an adaptive double-focusing method: Geophysics, **83**, no. 6, S579–S590, doi: 10.1190/geo2017-0796.1.
Tang, Y., 2009, Target-oriented wave-equation least-squares migration/inversion with phase-encoded Hessian: Geophysics, **74**, no. 6, WCA95–WCA107, doi: 10.1190/1.3204768.
Thorbecke, J. W., E. Slob, J. Brackenhoff, J. van der Neut, and K. Wapenaar, 2017, Implementation of the Marchenko method: Geophysics, **82**, no. 6, WB29–WB45, doi: 10.1190/geo2017-0108.1.
Valenciano, A. A., B. Biondi, and A. Guitton, 2006, Target-oriented wave-equation inversion: Geophysics, **71**, no. 4, A35–A38, doi: 10.1190/1.2213359.
van den Berg, P. M., 2021, Acoustic waves, *in* Forward and inverse scattering algorithms based on contrast source integral equations: John Wiley & Sons, Ltd., 79–179.
van der Neut, J., I. Vasconcelos, and K. Wapenaar, 2015a, On Green's function retrieval by iterative substitution of the coupled Marchenko equations: Geophysical Journal International, **203**, 792–813, doi: 10.1093/gji/ggv330.
van der Neut, J., K. Wapenaar, J. Thorbecke, and E. Slob, 2015b, Practical challenges in adaptive Marchenko imaging: 85th Annual International Meeting, SEG, Expanded Abstracts, 4505–4509, doi: 10.1190/segam2015-5791035.1.
van Groenestijn, G. J., and D. J. Verschuur, 2009, Estimating primaries by sparse inversion and application to near-offset data reconstruction: Geophysics, **74**, no. 3, A23–A28, doi: 10.1190/1.3111115.
Van IJsseldijk, J., and K. Wapenaar, 2020, Adaptation of the iterative Marchenko scheme for imperfectly sampled data: Geophysical Journal International, **224**, 326–336, doi: 10.1093/gji/ggaa463.
Wapenaar, C., and A. Berkhout, 1989, Elastic wavefield extrapolation: Redatuming of single and multi-component seismic data: Elsevier Science Publishers B.V.
Wapenaar, K., J. Brackenhoff, M. Dukalski, G. Meles, C. Reinicke, E. Slob, M. Staring, J. Thorbecke, J. van der Neut, and L. Zhang, 2021, Marchenko redatuming, imaging, and multiple elimination and their mutual relations: Geophysics, **86**, no. 5, WC117–WC140, doi: 10.1190/geo2020-0854.1.
Wapenaar, K., and M. Staring, 2018, Marchenko-based target replacement, accounting for all orders of multiple reflections: Journal of Geophysical Research: Solid Earth, **123**, 4942–4964, doi: 10.1029/2017JB015208.
Wapenaar, K., J. Thorbecke, J. van der Neut, F. Broggini, E. Slob, and R. Snieder, 2014, Marchenko imaging: Geophysics, **79**, no. 3, WA39–WA57, doi: 10.1190/geo2013-0302.1.
Willemsen, B., A. Malcolm, and W. Lewis, 2016, A numerically exact local solver applied to salt boundary inversion in seismic full-waveform inversion: Geophysical Journal International, **204**, 1703–1720, doi: 10.1093/gji/ggv547.
Ypma, F., and D. Verschuur, 2013, Estimating primaries by sparse inversion, a generalized approach: Geophysical Prospecting, **61**, 94–108, doi: 10.1111/j.1365-2478.2012.01095.x.
Yuan, S., N. Fuji, S. Singh, and D. Borisov, 2017, Localized time-lapse elastic waveform inversion using wavefield injection and extrapolation: 2-D parametric studies: Geophysical Journal International, **209**, 1699–1717, doi: 10.1093/gji/ggx118.
Zhang, L., J. Thorbecke, K. Wapenaar, and E. Slob, 2019, Transmission compensated primary reflection retrieval in the data domain and consequences for imaging: Geophysics, **84**, no. 4, Q27–Q36, doi: 10.1190/geo2018-0340.1.
Zhao, Z., and M. K. Sen, 2018, Fast image-domain target-oriented least-squares reverse time migration: Geophysics, **83**, no. 6, A81–A86, doi: 10.1190/geo2018-0033.1.
Zhou, H.-W., H. Hu, Z. Zou, Y. Wo, and O. Youn, 2018, Reverse time migration: A prospect of seismic imaging methodology: Earth-Science Reviews, **179**, 207–227, doi: 10.1016/j.earscirev.2018.02.008.

Biographies and photographs of the authors are not available.